

ORIGINAL ARTICLE

Numerical Investigation of Subcooled Boiling Heat Transfer in Helically-Coiled Tube

Luthfi A. F. Haryoko¹, Jundika C. Kurnia^{1*} and Agus P. Sasmito²¹Department of Mechanical Engineering, Universiti Teknologi PETRONAS, 32610 Seri Iskandar, Malaysia.

Phone: +605 368 7157; Fax: +605 365 6461

²Department of Mining and Materials Engineering, McGill University, 3450 University Street, Frank Dawson Adam Bldg, Montreal Quebec H3A 2A7 Canada

ABSTRACT – Subcooled boiling heat transfer in helically-coiled tubes offers better heat transfer performance than any other types of boiling processes due to its ability to capture high heat flux with a relatively low wall superheat. This study investigates turbulent subcooled forced convection boiling performances of water-vapour in a helically-coiled tube with various operating conditions i.e. operating pressure, heat, and mass flux. Developed CFD model is validated against previously published experimental results using the RPI model. The model is developed based on the Eulerian-Eulerian framework coupled with $k-\epsilon$ RNG turbulence model and Standard Wall-Function. A good agreement is found between numerical prediction and experimental counterpart for the bulk fluid temperature and non-dimensional length. The result indicates that the subcooled boiling heat transfer in a helically-coiled tube tends to improve heat transfer coefficient and pressure drop in the domain. Subcooled boiling starts at the inner side of the helically-coiled tube ($\phi=990^\circ$) due to the existence of secondary flow that comes from the coil curvature. Heat transfer coefficient and pressure drop increased with increasing heat flux and decreasing mass flux, and operating pressure. This is caused by the bubble movement and convective heat transfer phenomena in a helically-coiled tube. Finally, this study can provide a guideline for future research of the subcooled boiling in a helically-coiled tube.

ARTICLE HISTORYRevised: 8th Feb 2020Accepted: 13th Feb 2020**KEYWORDS**

Helically-coiled tubes; HTC, Numerical investigation, Pressure drop; RPI model, Subcooled boiling

NOMENCLATURE

<i>Symbol</i>		V_p	bubble volume, m ³
A_b	area of influence	K	empirical constant
A_i	interfacial area density, 1/m	<i>Greek alphabets</i>	
A_{if}	interfacial area concentration, 1/m	λ	diffusivity, m ² /s
C_p	specific heat, J/kg K	ρ	density, kg/m ³
d_{in}	inner tube diameter, m	ϕ	helical angle, °
d_o	outer tube diameter, m	τ	time period, s
d_p	average diameter of the bubble, m	$\bar{\tau}$	stress tensor
D	coil diameter, m	<i>Subscript</i>	
D_w	bubble departure diameter, m	C	convective heat transfer
f	bubble departure frequency, 1/s	cond	condensation heat transfer
F	interphase forces, N	E	evaporative heat transfer
g	standard gravity, m/s ²	i	interfacial
G	mass flux, kg/m ² s	j, l	liquid
h	coefficient of heat transfer, W/m ² K	g, k	gas
h_{jk}	heat of vaporization, J/kg	p	bubble
H	specific enthalpy, J/kg	Q	quenching heat transfer
k	heat conductivity, W/m K	sub	subcooled fluid
L_h	heated length, m	sat	saturated
\dot{m}	mass flow rate per volume, kg/m ³ .s	vap	vapour
N_w	nucleation density, sites/m ²	w	heated surface
\vec{n}	normal force, kg m/s ²	<i>Dimensionless components</i>	
P	operating pressure, MPa	C	interphase forces coefficient
p	helical pitch, m	Ja	Jacob number
q''	heat flux, W/m ²	Nu	Nusselt number
q	elements of heat flux, W/m ²	Pr	Prandtl number
S, Π	source term	Re	Reynolds number
T	temperature, K	x	vapour quality
ΔT	delta temperature, K	<i>Acronyms</i>	
$\vec{U}_{k,j}$	phase-weighted velocity, m/s	HT	heat transfer
\vec{v}	relative velocity, m/s	HTC	heat transfer coefficient

INTRODUCTION

The helically-coiled tube has been used in engineering applications including steam generators, boilers, mixer, cooling engines, and heat exchangers. It has high heat and mass transfer rate with a compact design. The helically-coiled tube has been studied by researchers worldwide as an outcome of the existence of secondary flow generated by the coil curvature [1–3]. Dean [4,5] was the first scholar who investigated the transport phenomena inside the helically-coiled tube. Subsequently, vast numbers of study, both experimentally [6,7] and numerically [8,9] have been reported. In most current studies on the helically-coiled tube, have been focused to scrutinize the single-phase heat transfer (HT) with only minor studies investigating two-phase flow HT inside the helical tube. Fsadni and Whitty and Naphon and Wongwises investigated the two-phase flow characteristics in a helically-coiled tube. It was reported that there was a lack of fundamental knowledge of two-phase flow and HT in a helically-coiled tube in comparison with the normal straight tube. Henceforth, there is a need to study the forced convection boiling HT inside the helical tube [10-11].

In the effort to further enhance the HT performance of helical tube, there is a proposal to utilise forced convection boiling HT in helically-coiled tube. This is driven by the fact that forced convection boiling HT offers much higher HT rate as compared to the single-phase counterpart [12]. Accordingly, several researches on it have been conducted and reported. Kong et al. [13] studied the subcooled boiling HT of R134a in a vertical helical tube with various operating conditions, including inlet subcooling, heat, and mass flux. It was found that the developed vapour phase consistently travels along the heated surface at the upward direction of the helical tube. Interestingly, the radial component force was negative, and it provided the augment of HT and the surface temperature difference in subcooled flow boiling. Additionally, there was a significant variation in the temperature distribution between the vertical and horizontal helical tube. However, there was no difference between both configurations in terms of the heat transfer coefficient (HTC), which is affected by secondary flow, velocity contour of the fluid flow, and bubble characteristics. Santini et al. [14] investigated forced convection boiling in a helically-coiled steam generator for the nuclear industry. The outcomes showed that HTC depends on the mass and heat flux in the HT for both nucleate and convective boiling. Furthermore, it was concluded that there were no significant contributions from coil curvature on the HT process during forced convection boiling. Meanwhile, the boiling HTC in a helically-coiled tube at high pressure with water as the main flow was experimentally examined by Xiao et al. [15]. The outcomes indicated that the pressure condition, heat and mass flux have a substantial contribution for the entire boiling HTC. When the heat flux and pressure in the system were increased, the HTC of subcooled and saturated nucleate boiling enhanced by several points. Meanwhile, the HTC of saturated convective boiling improved as the mass flux increased in the heat transfer phenomena. A numerical study of subcooled boiling in helically coiled heat exchanger under normal operating condition was conducted by Jo et al. [16]. They used both configurations between RPI wall and bulk boiling model in vertical tubes and compared them with the experimental case [17]. The result determined that the bulk boiling model inside the straight tube could anticipate better than RPI model in regards to the void fraction phenomenon. Thus, a bulk boiling model is used to study subcooled boiling in a helically-coiled tube. Abdous et al. [18] investigated flow boiling in a small helically-coiled tube at low vapour quality using CFD technique. The lowest and highest HTC in the simulation can be seen at the inner and bottom wall of the helically-coiled tube. Furthermore, the impact of coil diameter, tube diameter, and pitch were highlighted in the study. It showed that the HTC will be augmented at low vapour quality when the coil and tube diameters are decreasing, and the pitch is increasing. Boiling phenomenon inside the helically-coiled tube is more promising as compared to the straight pipe that comes from the secondary flow induced by centrifugal force [19]. In addition, subcooled boiling HT generate better HT efficiency than any other type of HT mode due to its behaviour to absorb better heat flux with a relatively small difference in temperature between the wall and fluid [20]. However, none of these studies had evaluated the effect of operating conditions on subcooled boiling HT at the helically-coiled tube using numerical prediction. Therefore, it is of interest to numerically evaluate the thermal-hydraulic performance of subcooled boiling HT inside the helically-coiled tube, which is one of the focuses of this study.

Based on the author's best knowledge, only two numerical studies are currently available on the investigation of the subcooled boiling HT in a helically-coiled tube. Furthermore, both studies focus only on the various geometrical properties and flow distributions using a bulk boiling model. Hence, there is a lack of studies on subcooled boiling HT in a helically-coiled tube. The current study investigates the subcooled boiling HT in the helically-coiled tube with the objective to evaluate the thermal-hydraulic performance in various operating parameters. The effect of heat flux, mass flux, and operating pressure are evaluated and discussed. A two-fluid RPI model is utilised to investigate the subcooled boiling phenomena in the helically-coiled tube. HTC and pressure drop are determined to evaluate flow behaviour and heat transfer phenomena. This research is proposed to provide an extensive performance analysis of the evaluated operating conditions.

MATHEMATICAL FORMULATION

A three-dimensional CFD model for subcooled boiling of a water-vapour turbulent flow in the helically-coiled tube is developed based on the Eulerian-Eulerian framework. The schematic description of the case under consideration is shown in Figure 1 and the features of the design and operating conditions are summarised in Table 1.

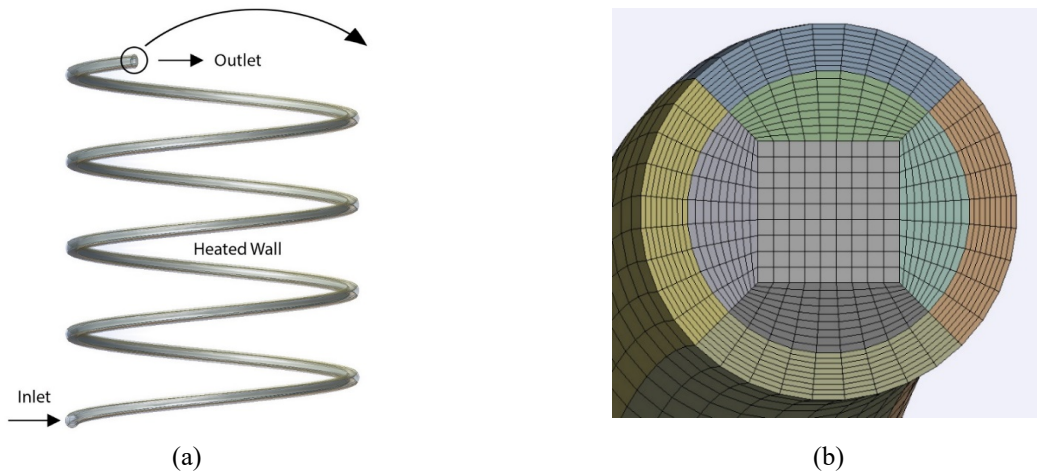


Figure 1. Schematic representation of helically-coiled tube from (a) side view and (b) cross-section of the mesh.

Table 1. Geometrical and operating parameters of the study.

Parameters	Value	Symbol
Inlet temperature (K)	303.15	T_{in}
Heat flux (W/m^2)	197×10^3	q''
Mass flux (kg/m^2s)	8.73×10^2	G
System pressure (MPa)	0.12	P
Inner tube diameter (m)	6×10^{-3}	d_{in}
Outer tube diameter (m)	8×10^{-3}	d_{out}
Coil diameter (m)	162×10^{-3}	D
Pitch (m)	5×10^{-2}	p
Heated length (m)	21.15×10^{-1}	L_h

Governing Equations

The Eulerian-Eulerian water-vapour model separately governs the mass, momentum, and energy equations for both phases. In this model, the interaction between the phases is combined with interphase exchange models. The governing equations for the liquid phase (j) and the vapour phase (k) are described as follows. The mass equations for phase j and k are:

$$\frac{\partial}{\partial t} (\alpha_j \rho_j) + \nabla \cdot (\alpha_j \rho_j \vec{v}_j) = \dot{m}_{kj} - \dot{m}_{jk} + S_j \tag{1}$$

$$\frac{\partial}{\partial t} (\alpha_k \rho_k) + \nabla \cdot (\alpha_k \rho_k \vec{v}_k) = \dot{m}_{jk} - \dot{m}_{kj} + S_k \tag{2}$$

where α_j , \vec{v}_j and ρ_j are the volume fraction, velocity, and density of the liquid phase, respectively. α_k , \vec{v}_k and ρ_k are the volume fraction, velocity, and density of the vapour phase, respectively. Meanwhile, \dot{m}_{jk} and \dot{m}_{kj} denotes the mass transfer between the liquid and vapour phases, S_j and S_k are the source term of both phases. The momentum balance for phase j and k yields:

$$\frac{\partial}{\partial t} (\alpha_j \rho_j \vec{v}_j) + \nabla \cdot (\alpha_j \rho_j \vec{v}_j \vec{v}_j) = - \vec{\alpha}_j \nabla p + \nabla \cdot \bar{\bar{\tau}}_j + \alpha_j \rho_j \vec{g} + \dot{m}_{kj} \vec{v}_{kj} - \dot{m}_{jk} \vec{v}_{jk} + \bar{F}_{kj} \tag{3}$$

$$\frac{\partial}{\partial t} (\alpha_k \rho_k \vec{v}_k) + \nabla \cdot (\alpha_k \rho_k \vec{v}_k \vec{v}_k) = - \vec{\alpha}_k \nabla p + \nabla \cdot \bar{\bar{\tau}}_k + \alpha_k \rho_k \vec{g} + \dot{m}_{jk} \vec{v}_{jk} - \dot{m}_{kj} \vec{v}_{kj} + \bar{F}_{jk} \tag{4}$$

where \vec{v}_{jk} and \vec{v}_{kj} are the interphase velocities, \bar{F}_{jk} and \bar{F}_{kj} are the interphase forces that are included in the model, p is the pressure shared by all phases and $\bar{\bar{\tau}}$ is the stress tensor. The energy equation for phase j and k can be formulated as:

$$\frac{\partial}{\partial t} (\alpha_j \rho_j H_j) + \nabla \cdot (\alpha_j \rho_j \vec{v}_j H_j) = \nabla \cdot [\alpha_j k_j (\nabla T_j)] + q_{ji} + (\dot{m}_{jk} H_{jk} - \dot{m}_{kj} H_{kj}) \tag{5}$$

$$\frac{\partial}{\partial t} (\alpha_k \rho_k H_k) + \nabla \cdot (\alpha_k \rho_k \vec{v}_k H_k) = \nabla \cdot [\alpha_k k_k (\nabla T_k)] + q_{ki} + (\dot{m}_{kj} H_{kj} - \dot{m}_{jk} H_{jk}) \tag{6}$$

where H_j and H_k is the specific enthalpy of both phases, q_{ji} and q_{ki} is the interfacial HT to the liquid and vapour phase which equal to $q_{ki} = 0$, H_{jk} and H_{kj} are the interphase enthalpies due to phase change for vapour condensation and liquid evaporation, respectively.

RPI Model

The concept of this method is utilised to define the adjacent-wall heat exchange of the subcooled boiling condition [21]. The overall heat flux from the heated surface to the water is distributed into several sectors. The sectors include the single-phase convection heat flux (q_C), the wall quenching heat flux (q_Q), and the evaporation heat flux (q_E).

$$q_W = q_C + q_Q + q_E \quad (7)$$

The single-phase convection heat flux, q_C refers to the form of convective HT between the water and the tube wall throughout the domain. Liquid near the wall is heated until its saturation point is reached. This phenomenon occurs in the area of the wall which is covered with liquid. Therefore, single-phase convection heat flux is expressed as,

$$q_C = h_c(T_w - T_j)(1 - A_b) \quad (8)$$

where h_c is single-phase HTC, T_w is the temperature at the wall while T_j is the temperature of the liquid and A_b is the ratio of the adjacent wall that is shielded by nucleate bubbles. A_b is based on the function of the departure diameter and the nucleate site density which can be predicted by:

$$A_b = \min\left(1, K \frac{N_w \pi D_w^2}{4}\right) \quad (9)$$

where the value of empirical constant K is given by Del Valle and Kenning formula [22].

$$K = 4.8 e^{\left(\frac{Ja_{sub}}{80}\right)} \quad (10)$$

and Ja_{sub} is the subcooled Jacob number interpreted as in Eq. (11).

$$Ja_{sub} = \frac{\rho_j C_{pj} \Delta T_{sub}}{\rho_k h_{jk}} \quad (11)$$

where $\Delta T_{sub} = T_{sat} - T_j$ is the subcooling temperature, C_{pj} is the specific heat of the liquid phase, and h_{jk} is the heat of vapourisation. The wall quenching heat flux, q_Q is the HT (forced convection) that occurred when the heat flux of the wall transfer the heat to the cooler liquid in order to recover the departed bubble at the heated wall vicinity.

$$q_Q = \frac{2k_j}{\sqrt{\pi\lambda_j\tau}} A_b (T_w - T_j) \quad (12)$$

where τ , k_j , and λ_j are the time period, heat conductivity, and diffusivity of the liquid phase respectively. The evaporation heat flux, q_E is caused by the phase change process from a liquid into vapour during bubble nucleation. It is calculated as the hidden heat transported over by the bubble detachment from the surface. q_E is described as Eq. (13).

$$q_E = V_p N_w f \rho_k h_{jk} \quad (13)$$

where $V_p = \frac{\pi D_w^3}{6}$ is the number of bubbles which depends on the departure diameter and D_w is the bubble departure diameter, given by Tolubinsky finding [23].

$$D_w = \min\left(0.0006 \cdot e^{\left(\frac{\Delta T_{sub}}{45}\right)}, 0.0014\right) \quad (14)$$

N_w is the nucleation density, given by Lemmert and Chawla correlation [24].

$$N_w = 210^{1.805} (T_w - T_{sat})^{1.805} \quad (15)$$

and f is the bubble departure frequency, given by Cole equation [25].

$$f = \frac{1}{T} = \sqrt{\frac{4g(\rho_j - \rho_k)}{3D_w\rho_j}} \quad (16)$$

where g is the standard gravity.

Interphase heat and mass transfer

The phase change of subcooled boiling HT is associated with the evaporation close to heated surface and condensation in the primary flow. When the bubbles leave the adjacent surface and travel to the primary flow, the condensation is achieved. The condensation HT can be formulated as:

$$\dot{q}_{ji} = \dot{q}_{cond} = h_{ji}A_i(T_{sat} - T_j) \tag{17}$$

where h_{ji} is interfacial HTC defined by $h_{ji} = Nuk_j/d_p$, d_p is the bubble diameter and A_i is interfacial area density. The value of Nu is predicted by the equation developed by Ranz-Marshall [26]:

$$Nu = 2 + 0.6 Re_k^{1/2} Pr_l^{1/3} \tag{18}$$

where Re_k is the Reynolds number that comes from the dispersed phase diameter and Pr_l is the Prandtl number of the continuous phase. In this study, the bubbles fixed at saturated temperature and the amount of mass transfer from the system is given by:

$$\dot{m}_{kj} = \dot{m}_{cond} = \max\left(\frac{\dot{q}_{cond}}{h_{jk}}, 0\right) \tag{19}$$

The bubble diameter, d_p defines as a role of the local subcooling. This model is utilised to measure d_p .

$$d_p = \begin{cases} \max\left[1.0 \times 10^{-5}, d_{min} \exp\left(\frac{-K(\Delta T_{sub} - \Delta T_{max})}{d_{min}}\right)\right] & \Delta T_{sub} > 13.5K \\ d_{max} - K(\Delta T_{sub} - \Delta T_{min}) & \Delta T_{sub} \leq 13.5K \end{cases} \tag{20}$$

where $d_{min} = 0.000015m$, $d_{max} = 0.001m$, $\Delta T_{min} = 0 K$, $\Delta T_{max} = 13.5 K$, $K = \frac{d_{max} - d_{min}}{\Delta T_{max} - \Delta T_{min}}$. The mass flow rate of vapour bubbles is calculated by:

$$\dot{m}_{jk} = \dot{m}_{vap} = \frac{\pi D_w^3}{6} \rho_k f N_w \tag{21}$$

Interphase momentum transfer

The interphase momentum transfer is determined by the interphase forces. The forces include the drag, lift, wall lubrication, and the turbulent dispersion force. The virtual mass force is ignored as the secondary phase in the subcooled forced convection boiling has no accelerative motion in the study. The movement of the bubble is resisted by the drag force. The drag force is equivalent to the slip velocity between the primary and secondary phase. The correlation of drag force is expressed as:

$$F_D = \frac{C_D \mu_j A_{if} Re}{8d_p} (\vec{v}_k - \vec{v}_j) \tag{22}$$

where C_D is the coefficient of drag, calculated by Ishii [27] correlation, μ_j is the viscosity of the water, A_{if} is the interfacial area concentration.

The lift force on vapour phase is induced by velocity gradient and vortex generation in the liquid phase domain or shear flow. Vapour bubbles emerge in the fluid flow due to the relative motion of both phases in a perpendicular direction. The lift force basic correlation based on Drew and Lahey [28] is formulated as:

$$\vec{F}_L = -C_L \rho_j \alpha_k (\vec{v}_j - \vec{v}_k) \times (\nabla \times \vec{v}_j) \tag{23}$$

where C_L is the coefficient of lift developed by Moraga formulation [29]. The difference of hydrodynamic pressure between bubbles and liquid flow in the vicinity of the wall causes the wall lubrication force. The wall lubrication forces drive away the vapour phase from the wall. The formulation of this force is expressed as:

$$\vec{F}_{wl} = C_{wl} \rho_j \alpha_k |\vec{v}_j - \vec{v}_k|^2 \vec{n}_w \tag{24}$$

where C_{wl} is the coefficient of wall lubrication proposed by Antal et al. [30] model, \vec{v}_j and \vec{v}_k are the velocity constituent between both phases tangential to the wall, and \vec{n}_w is the normal force from the wall.

The turbulent dispersion force is one of the impacts that cause for the interphase turbulent momentum transfer. The force operates as a turbulent diffusion in vapour phase and holds a vital role in pushing the bubbles away from the adjacent wall into liquid flow. Lopez de Bertodano [31] proposed the correlation for the model and is expressed as follows:

$$\vec{F}_{td,j} = -\vec{F}_{td,k} = C_{TD} \rho_j k_j \nabla \alpha_k \tag{25}$$

where $C_{TD} = 1$, which is a default setting for a user-modifiable constant, k_j is the turbulent kinetic energy of the liquid phase, and $\nabla\alpha_k$ is the gradient of vapour volume fraction.

Turbulence model

Turbulence model is employed in this study according to the similar case in the single-phase condition [32]. Nonetheless, some additional source terms are estimated into the secondary phase in the multiphase turbulence equations. k- ϵ RNG model is chosen in this particular case based on Ahmed et al. [33] study. In order to accommodate low Reynolds number effects, this model is principally relative on local turbulent viscosity. k- ϵ RNG supports extra term R_ϵ in the transport equation of the model, which includes effective viscosity [34]. In the modelling, the model proposed some variations to include the turbulence of the secondary phase in the k- ϵ equations. Standard wall-function is being adopted in the model by employing y^+ values above 11.225 to capture the phenomenon at the wall boiling surface.

In the turbulence model, it is usually spotted in the flow field that the wakes are generated behind vapour when the large or medium-sized of vapour phase is flowing throughout the domain. The influence of wakes could produce additional turbulence in the system. In order to calculate for additional turbulence by liquid droplets, the turbulent interaction model is used. The importance of the liquid droplets is depicted by source terms (Π_{k_j} and Π_{ϵ_j}) whose form rely on the model chosen. Troshko-Hassan [35] proposed formula to measure for the turbulence of the liquid droplets in the k- ϵ equations. In the mixture turbulence models, the correlation is expressed as follow:

$$\Pi_{k_m} = C_{ke} \sum_{k=1}^M K_{kj} |\vec{U}_k - \vec{U}_j|^2 \quad (26)$$

$$\Pi_{\epsilon_m} = C_{td} \frac{1}{\tau_k} \Pi_{k_m} \quad (27)$$

where $C_{ke} = 0.75$ and $C_{td} = 0.45$ is determined by default, τ_k is the time-specific that caused by turbulence illustrated as:

$$\tau_k = \frac{2C_{VM}d_k}{3C_D|\vec{U}_k - \vec{U}_j|} \quad (28)$$

Constitutive Relations

The equilibrium quality corresponds to the vapour flow fraction only if there is a thermodynamic equilibrium exists between the phases. Since the equilibrium quality is prescribed in terms of the enthalpy of the fluid, the value may be greater than one and less than zero. Under these conditions, the equilibrium quality may be considered as a measure of the degree of the fluid's subcooling or superheat but cannot be used to determine the fluid state.

$$x = \frac{h - h_j}{h_{jk}} \quad (29)$$

where x is vapour quality, h is the enthalpy of fluid, and h_j is the enthalpy of fluid at saturation value.

Boundary Conditions

The following boundary conditions have been adopted to simulate the study of subcooled boiling HT inside the helically-coiled tube: constant velocity and temperature is prescribed at the inlet. For the outlet, we put the zero-gauge pressure and zero streamwise temperature gradient. For the heated wall, we specified the no-slip condition and constant wall heat flux [36].

NUMERICAL METHODOLOGY

The numerical investigation is performed using CFD software package (ANSYS Fluent). Thermo-physical characteristics of the water are obtained from the NIST database [37] and incorporated as piecewise-linear functions in the solver. For the vapour phase, the temperature properties are set at the saturation value. The simulation is conducted by using Coupled algorithm with volume fraction for determining the pressure-velocity coupling in the domain. For spatial discretization, the default setting is applied in the Gradient part. The QUICK option is used to calculate the volume fraction terms. Other discretisation settings are settled with Second Order Upwind. The convergence criteria for all the parameters are set at 10^{-5} and the tolerance of the ratio of mass from rate imbalance is below 1%.

Mesh independent study is conducted to provide mesh independent result by consistently improving the mesh elements as shown in Table 2. The results indicated that there is no substantial difference for quality and bulk temperature when the mesh is increased beyond 729k elements. Thus, this mesh configuration is selected for the rest of the study.

Table 2. Mesh independent study for the present model.

Case	Outlet bulk temperature (K)	Outlet quality (x)	Percentage difference (%)
Experimental	375.87	-0.00005	-
Simulation (225k mesh)	382.5	0.008601	1.74%
Simulation (441k mesh)	382.19	0.008017	1.66%
Simulation (729k mesh)	382.33	0.008285	1.69%
Simulation (1089k mesh)	382.31	0.008245	1.69%
Simulation (1521k mesh)	382.3	0.008227	1.68%

RESULTS AND DISCUSSION

In an attempt to evaluate the behaviour of subcooled boiling within the helical tube, the numerical prediction is performed for subcooled boiling in the various operating conditions including various operating pressure, mass and heat flux. The HTC and pressure drop for each configuration are evaluated and discussed.

Model Validation

For model validation purposes, numerical simulation is conducted based on the experimental case of Hardik and Prabhu [38] using the RPI model. The result from the numerical model is compared with the experimental investigation to ensure accuracy and validity of the developed model. As shown in Figure 2, good agreement is shown between numerical simulations and experimental study of the bulk fluid temperature with regards to the non-dimensional length of the helically-coiled tube. Overall, it is found that the relative error for the bulk fluid temperature is less than 2%. It can be seen that the inlet temperature for both studies is very close to 315K. When the temperature increases inside the tube, there is a small deviation between the numerical and experimental result. This result gives a firm indication that the developed model can predict the experimental result relatively well. In addition, the developed model requires less time to compute as compared with the bulk boiling model. Consequently, the developed model using the RPI model is the first study investigating the subcooled boiling inside the helically-coiled tube.

Variations of Vapour Volume Fraction Along the Coiled Tube

The contours of vapour volume fraction at a designated location along the coiled tube are shown in Figure 3. It is observed that the boiling starts at the inner wall of the tube ($\phi=990^\circ$). The coil curvature induces the secondary flow [18]. The secondary flow enhances fluid mixing and convection HT close by the outer wall [39]. Due to this behaviour, the inner wall of the tube has a higher temperature to cause boiling faster than any other parts of the wall. The result is more obvious at $\phi=1170^\circ$ as presented in Figure 3. The farther fluid flowing downstream of the tube, vapour presence become more pronounced which could be seen by higher vapour volume fraction at $\phi=1350^\circ$ and $\phi=1440^\circ$. This process occurs due to bulk temperature has reached saturation point and more vapour generation at the wall.

Figure 4 demonstrates the secondary flow contours and vectors at various angles inside the helical tube. It is shown that the secondary flow is more significant in the downstream area. The secondary flow is more obvious at the inner side of the wall as a result of the centrifugal effect from coil curvature that generates substantial pressure difference in the main flow. The velocity at the axial direction and centrifugal forces around the heated wall is almost nil hence secondary flow creates equilibrium condition in momentum balance [40].

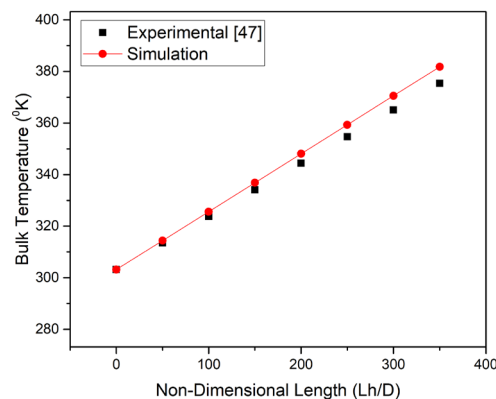


Figure 2. The bulk fluid temperature with the non-dimensional length between the present study and experimental investigation.

Heat Transfer Coefficient and Vapour Quality along the Coiled Tube

Figure 5 shows the relationship between HTC and vapour quality along the coiled tube. The primary HT process in the subcooled boiling is the nucleate bubble that comes from nucleation spots at the wall [15]. The better HT will occur when there are more bubbles generated in the tube. These nucleate bubbles correspond with the outlet vapour quality. It means that HTC will increase by increasing the outlet vapour quality along the helically-coiled tube. The trend shows

that HTC keeps increasing from the quality (-0.06-0.01) in the helically-coiled tube. At the quality around -0.06, the HTC is below 10,000 W/m²K. The bubble nucleation is generating at the wall which could affect the HTC value across the helically-coiled tube. When the quality reaches -0.02, the HTC presents an improvement from the previous one. It is due to the active nucleation site in the heated wall starts to grow which corresponds to the bubble nucleation development inside the helically-coiled tube. The HTC occupies the highest spot for this operating condition in the position of quality above zero. From this phenomenon, it can be interpreted that the condition is no longer in the subcooled boiling region. Furthermore, the HT process will be more severe than any other boiling region for this particular case. The HTC in this position is around 20,000 W/m²K.

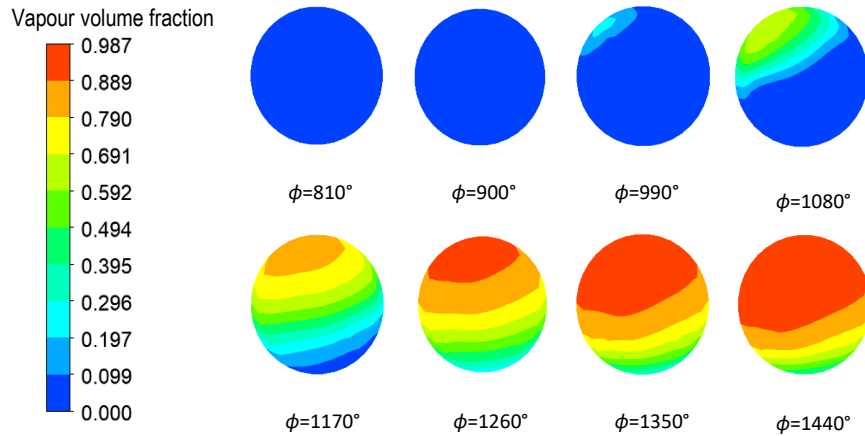


Figure 3. Vapour volume fraction contours at various angles in coiled tube.

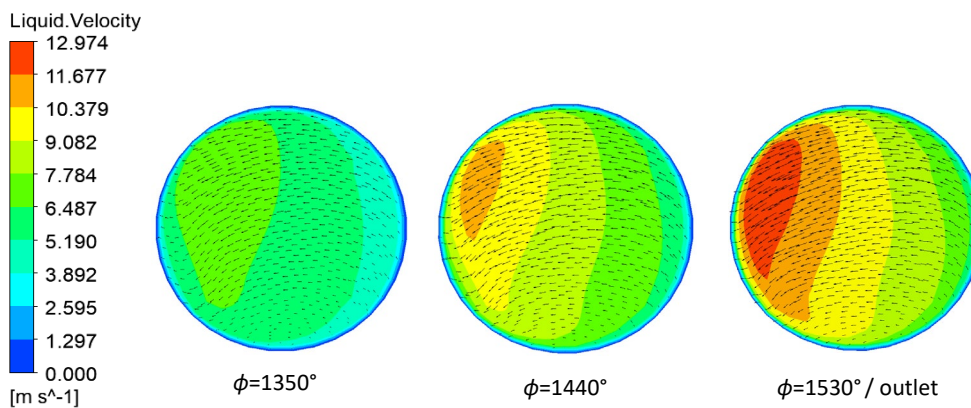


Figure 4. Secondary flow contours and vectors at different angles inside the helical tube.

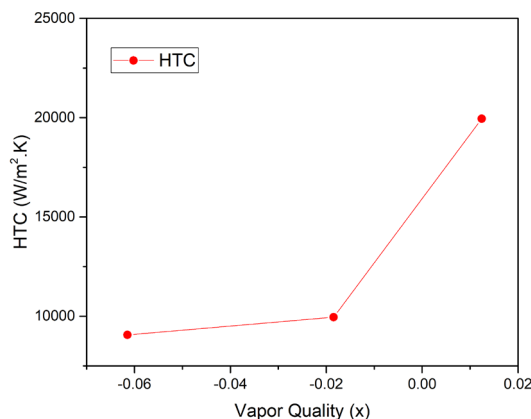


Figure 5. The relationship between the HTC and vapour quality along the helically-coiled tube.

Pressure Distribution Along the Coiled Tube

Figure 6 shows the pressure distribution along the coiled tube. It is shown that the pressure distribution tends to decrease in the developed model. This trend is in-line with the result by Cioncolini et al. [41] study, which defined the pressure distribution along the coiled tube. In their literature, it tends to decrease systematically due to Darcy’s Law that applies for pressure distribution in the pipe. According to Darcy’s Law, the high pressure will move into a lower position,

which means that the inlet condition should have a higher-pressure value than the outlet condition. This behaviour is considered to have a uniform trend with the present study as shown in Figure 6. From this trend, the pressure drop of this study is estimated to be around 66.796 kPa. Thus, the correlation between the pressure drop and HTC in subcooled boiling in the tube presents a linear agreement. The HTC increases with increasing pressure drop due to the presence of secondary flow induced by coil curvature. Also, this reported pressure drop could be the future reference to determine the subcooled boiling process inside the helically-coiled tube.

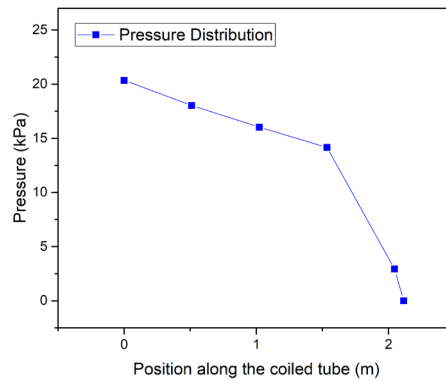


Figure 6. The pressure distribution along the helically-coiled tube.

Effect of Heat Flux on HTC and Pressure Drop in Subcooled Boiling

The effects of heat flux on HTC and two-phase flow pressure drop in subcooled boiling regions for helically-coiled tube are displayed in Figure 7. The HTC distribution with the vapour quality in the helically-coiled tube is shown in Figure 7(a). There is a strong increment of HTC that can be observed by the increase of vapour quality from -0.08 to 0.03. Moreover, HTC increases when the heat flux is improved from 145 kW/m² to 230 kW/m². The bubble nucleation contributes to the improvement of the HT process. Heat flux prompts higher nucleation density. Thus, the allocation of boiling HTC in the subcooled boiling area enhances when the heat flux rises. Highest HTC is achieved at heat flux of 197 kW/m² with the vapour quality of 0.012. It occurs due to a small difference between the inner wall and bulk fluid temperature induced by low wall superheat. In addition, the small temperature difference is influenced by the coil curvature from the helically-coiled tube. The pressure drop profile with the outlet quality in the helically-coiled tube is shown in Figure 7(b). There is a linear correlation between the increment of heat flux and pressure drop. Moreover, the pressure drop increases when the outlet quality is improved. Pressure drop for heat flux 145 kW/m² and 197 kW/m² is increased from 60 kPa to 67 kPa respectively. The increment of pressure drop has observed at the outlet quality 0.001 and 0.009 respectively. It is due to the intensity of nucleate boiling is higher enough to generate higher pressure drop at the high heat flux. Therefore, the highest pressure drop of 90 kPa in the system is observed at the corresponding heat flux of 230 kW/m². It occurs due to the wall superheat is large enough to produce bubbles while the outlet quality is at 0.013. More bubbles in the tube correspond with the high-pressure drop. It is expected since higher HT produces more bubble which in turn lead to higher pressure drop. Hence, HTC and pressure drop increases as the heat flux increases.

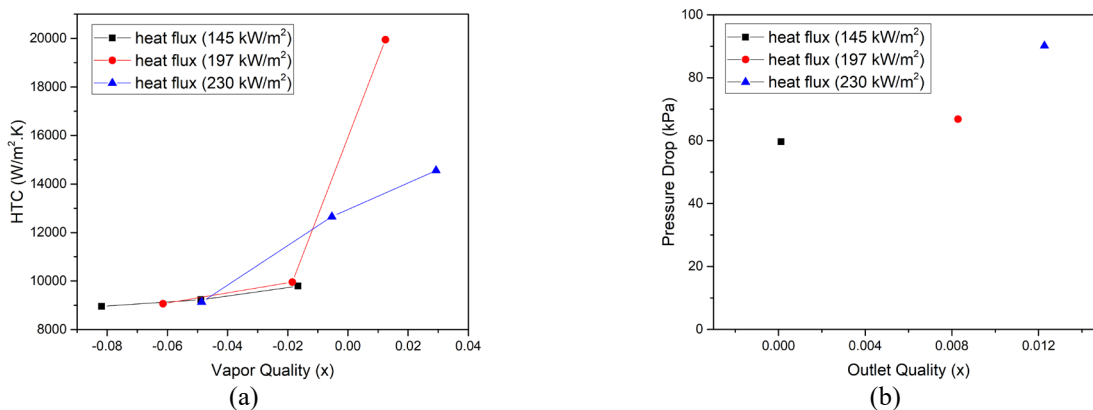


Figure 7. Impact of heat flux in the subcooled boiling region: (a) HTC vs vapour quality and (b) pressure drop vs. outlet quality.

Effect of Mass Flux on HTC and Pressure Drop in Subcooled Boiling

The effects of mass flux on HTC and two-phase flow pressure drop in subcooled boiling regions at helically-coiled tube are illustrated in Figure 8. The HTC distribution with the vapour quality in the helically-coiled tube is shown in Figure 8(a). The HTC slightly enhances with the vapour quality varied in a range of -0.08 to 0.04. Subcooled condition can be achieved by increasing the mass flux from 665 kg/m².s to 1081 kg/m².s. The phenomenon is dominantly occurred due to convective HT in the tube. This mechanism depends on the degree of high subcooling condition. Hence, the

convection HT plays a major role when the mass flux is augmented. Highest HTC is obtained in vapour quality of 0.012 when the mass flux is $873 \text{ kg/m}^2\cdot\text{s}$. It occurs due to wall superheat is at a sufficient level to generate vapour bubbles. Initially, few nucleation sites are enabled, and HTC still relies heavily on mass flux. The pressure drop profile with the outlet quality in the helically-coiled tube is shown in Figure 8 (b). The pressure drop decreases as the mass flux increases. The increased mass flux causes a decrease in outlet vapour quality. Also, the pressure drop has a linear increase with vapour quality. It is due to the increment of bulk temperature that comes from the declining of mass flux. It is expected that the formation of the bubbles, which usually under higher bulk temperature will lead to the increase of pressure drop. Therefore, the largest pressure drop of 75 kPa is observed when the mass flux is at $665 \text{ kg/m}^2\cdot\text{s}$. At this point, the outlet quality is at 0.019. It occurs due to the pressure drop is not a function of mass flux. The effect of mass flux is not essentially significant rather than heat flux for generating pressure drop. Hence, HTC and pressure drop are inversely proportional to the increase in mass flux.

Effect of Operating Pressure on HTC and Pressure Drop in Subcooled Boiling

The effects of operating pressure on HTC and two-phase flow pressure drop in subcooled boiling regions at helically-coiled tube are demonstrated in Figure 9. The HTC distribution with the vapour quality in the helically-coiled tube is shown in Figure 9(a). The increase of operating pressure causes higher vapour density, which leads to a decrease in the average velocity of the fluid. The decrease in average fluid velocity leads to the lower convective HT process. Also, the enhanced wettability due to higher operating pressure decreases the bubble mechanism in the helical pipe wall. Highest HTC is achieved at an operating pressure of 0.12 MPa with the vapour quality of 0.012. It is occurred due to HTC increase as the vapour quality increases. However, the enhancement of HTC is inversely proportional to the operating pressure. The pressure drop profile with the outlet quality in the helically-coiled tube is shown in Figure 9(b). It is found that low operating pressure correlates to high-pressure drop. At constant temperature, low operating pressure correlates to high vapour quality. The influence of operating pressure in vapour quality is one of the factors that determines the pressure drop in subcooled boiling. These characteristics are critical in bubble distribution and nucleate boiling. Pressure drop in the subcooled boiling condition is more substantial at low operating pressure due to heat exchange capacity is increased by decreasing latent heat. The highest pressure drop of 67 kPa in the tube is observed at the corresponding operating pressure of 0.12 MPa. The outlet quality for the corresponding operating pressure is 0.008. However, the pressure drop at 0.48 MPa is in a higher position compared with the pressure drop at 0.24 MPa while the outlet quality is not showing the same pattern for both configurations. This is due to the subcooled boiling condition in the helically-coiled tube, which could contribute to the increase of pressure drop. Hence, HTC and pressure drop increase as the operating pressure decreases.

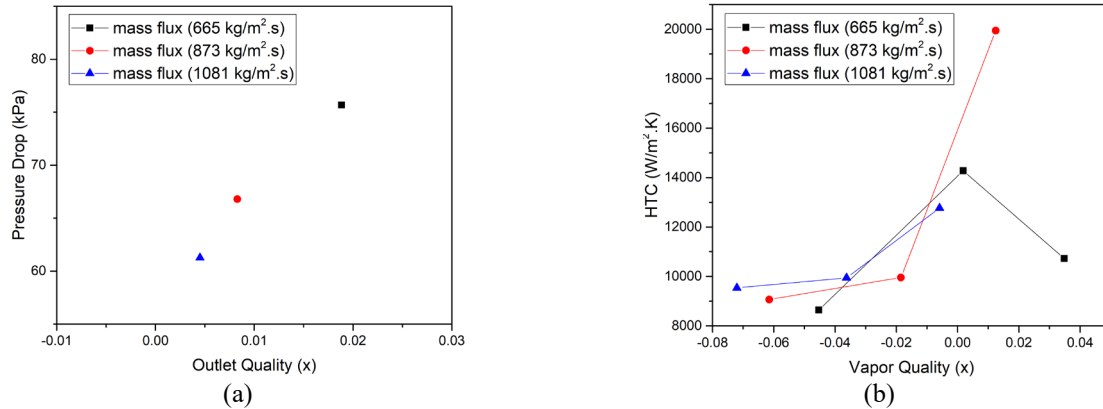


Figure 8. Impact of mass flux in the subcooled boiling region: (a) HTC vs vapour quality and (b) pressure drop vs. outlet quality.

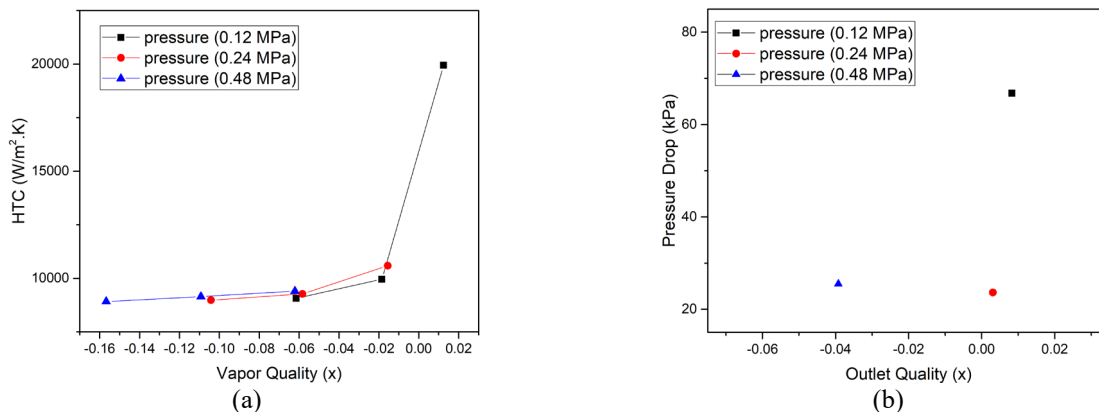


Figure 9. Impact of operating pressure in the subcooled boiling region: (a) HTC vs vapour quality and (b) pressure drop vs. outlet quality.

CONCLUSION

Numerical investigation of subcooled boiling HT inside the helically-coiled tube has been conducted using a 3D CFD model. The result of HTC and pressure drop have been evaluated. Using the developed model, the variations of vapour volume fraction along the coiled tube at different helical angles have been studied and discussed. It is found that the boiling starts at the inner side of the tube, which is caused by the existence of secondary flow. The secondary flow in coil curvature enhances fluid mixing and convective HT close to the outer wall. The main HT in the subcooled boiling is caused by the bubble nucleation which highly depends upon the nucleation spots. The gravity and centrifugal force also contribute to increase the vapour presence at the adjacent heated wall. The HTC can reach up to 20,000 W/m²K at the vapour quality above zero. Pressure distribution has been evaluated as well. It is found that Darcy's Law is the governing factor of pressure distribution where the pressure in the inlet is higher than the outlet. The pressure drop of this system is calculated at 66.796 kPa. The impact of heat flux to HTC and pressure drop during subcooled boiling is significant. An escalation of heat flux leads to the enhancement of both HTC and pressure drop. Higher heat flux causes faster bubble nucleation. The impact of mass flux in subcooled boiling HT is also essential for HTC improvement. It is found that the convective HT is the main HT process during the variation of mass flux. While the pressure drop gives the opposite result while the mass flux is augmented. This is occurred due to pressure drop is not a function of mass flux. The impact of operating pressure in subcooled boiling HT is different than other parameters that have been considered. When the operating pressure rises, the HTC and pressure drop deteriorate. This is because of the convective HT is not prominent that comes from the enhancement of vapour density.

Based on this study, the subcooled boiling in the helically-coiled tube should be further scrutinised in more details to give more explanation about the boiling processes that occur in a helically-coiled tube. The effect of various cross-sections geometries and enhancement methods could be the direction for future research of subcooled boiling within a helically-coiled tube.

ACKNOWLEDGEMENT

The authors gratefully acknowledge the facility and financial support from the Ministry of Higher Education Malaysia through Fundamental Research Grant Scheme (FRGS) no FRGS/1/2018/TK07/UTP/02/8 (CS: 015MA0-028).

REFERENCES

- [1] Guo L-J, Feng Z-P, Chen X-J. Pressure drop oscillation of steam-water two-phase flow in a helically coiled tube. *International Journal of Heat and Mass Transfer*. 2001; 44: 1555-1564.
- [2] Jayakumar JS, Mahajani SM, Mandal JC, Vijayan PK, Bhoi R. Experimental and CFD estimation of heat transfer in helically coiled heat exchangers. *Chemical Engineering Research and Design*. 2008; 86(3): 221-232.
- [3] Vashisth S, Kumar V, Nigam KDP. A review on the potential applications of curved geometries in process industry. *Industrial & Engineering Chemistry Research*. 2008; 47(10): 3291-3337.
- [4] Dean WR. Note on the motion of fluid in a curved pipe. *The London, Edinburgh, and Dublin Philosophical Magazine and Journal of Science*. 1927; 4(20): 208-223.
- [5] Dean WR. The stream-line motion of fluid in a curved pipe (Second paper). *The London, Edinburgh, and Dublin Philosophical Magazine and Journal of Science*. 1928; 5(30): 673-695.
- [6] Naphon P. Experimental investigation the nanofluids heat transfer characteristics in horizontal spirally coiled tubes. *International Journal of Heat and Mass Transfer*. 2016; 93: 293-300.
- [7] Pawar SS, Sunnapwar VK. Experimental studies on heat transfer to Newtonian and non-Newtonian fluids in helical coils with laminar and turbulent flow. *Experimental Thermal and Fluid Science*. 2013; 44: 792-804.
- [8] Kurnia JC, Sasmito AP, Mujumdar AS. Evaluation of the heat transfer performance of helical coils of non-circular tubes. *Journal of Zhejiang University-SCIENCE A*. 2011; 12(1): 63-70.
- [9] Kurnia JC, Sasmito AP, Mujumdar AS. Laminar heat transfer performance of power law fluids in coiled square tube with various configurations. *International Communications in Heat and Mass Transfer*. 2014; 57: 100-108.
- [10] Fsadni AM, Whitty JPM. A review on the two-phase heat transfer characteristics in helically coiled tube heat exchangers. *International Journal of Heat and Mass Transfer*. 2016; 95: 551-565.
- [11] Naphon P, Wongwises S. A review of flow and heat transfer characteristics in curved tubes. *Renewable and Sustainable Energy Reviews*. 2006; 10(5): 463-490.
- [12] Ramasamy D, Kadirgama K, Rahman MM, Zainal ZA. Analysis of compressed natural gas burn rate and flame propagation on a sub-compact vehicle engine. *International Journal of Automotive and Mechanical Engineering*. 2015; 11: 2405-2416.
- [13] Kong L, Han J, Chen C, Xing K, Lei G. An experimental study on subcooled flow boiling heat transfer characteristics of R134a in vertical helically coiled tubes. *Experimental Thermal and Fluid Science*. 2017; 82: 231-239.
- [14] Santini L, Cioncolini A, Butel MT, Ricotti ME. Flow boiling heat transfer in a helically coiled steam generator for nuclear power applications. *International Journal of Heat and Mass Transfer*. 2016; 92: 91-99.
- [15] Xiao Y, Hu Z, Chen S, Gu H. Experimental investigation of boiling heat transfer in helically coiled tubes at high pressure. *Annals of Nuclear Energy*. 2018; 113: 409-419.

- [16] Jo JC, Kim WS, Choi C-Y, Lee YK. Numerical simulation of subcooled flow boiling heat transfer in helical tubes. *Journal of Pressure Vessel Technology*. 2009; 131(1): 011305.
- [17] Owhadi A, Bell KJ, Crain B. Forced convection boiling inside helically-coiled tubes. *International Journal of Heat and Mass Transfer*. 1968; 11: 1779-1793.
- [18] Abdous MA, Holagh SG, Saffari H. Numerical investigation of flow boiling heat transfer in helically coiled tube under constant heat flux. *Thermal Science and Engineering*. 2018; 1: 1-18.
- [19] Hardik BK, Prabhu SV. Heat transfer distribution in helical coil flow boiling system. *International Journal of Heat and Mass Transfer*. 2018; 117: 710-728.
- [20] Cheung SCP, Vahaji S, Yeoh GH, Tu JY. Modeling subcooled flow boiling in vertical channels at low pressures – Part 1: Assessment of empirical correlations. *International Journal of Heat and Mass Transfer*. 2014; 75: 736-753.
- [21] Kurul N. On the modeling of multidimensional effects in boiling channels. *ANS. Proc. National Heat Transfer Con. Minneapolis, Minnesota, USA*. 1991.
- [22] Del Valle VH, Kenning DBR. Subcooled flow boiling at high heat flux. *International Journal of Heat and Mass Transfer*. 1985; 28(10): 1907-1920.
- [23] Tolubinsky VI, Kostanchuk DM. Vapour bubbles growth rate and heat transfer intensity at subcooled water boiling. *Proceedings of the 4th International Heat Transfer Conference*. 1970; 5(B-2): 1-8.
- [24] Lemmert M, Chawla JM. Influence of flow velocity on surface boiling heat transfer coefficient. *Heat Transfer in Boiling*. 1977; 237: 247.
- [25] Cole R. A photographic study of pool boiling in the region of the critical heat flux. *AIChE Journal*. 1960; 6(4): 533-538.
- [26] Ranz WE, Marshall WR. Evaporation from drops. *Chemical Engineering Progress*. 1952; 48(3): 141-146.
- [27] Ishii M. Two-fluid model for two-phase flow. *Multiphase Science Technology*. 1990; 5(1-4): 1-63.
- [28] Drew DA, Lahey RT. Application of general constitutive principles to the derivation of multidimensional two-phase flow equations. *International Journal of Multiphase Flow*. 1979; 5(4): 243-264.
- [29] Moraga FJ, Bonetto FJ, Lahey RT. Lateral forces on spheres in turbulent uniform shear flow. *International Journal of Multiphase Flow*. 1999; 25(6): 1321-1372.
- [30] Antal SP, Lahey RT, Flaherty JE. Analysis of phase distribution in fully developed laminar bubbly two-phase flow. *International Journal of Multiphase Flow*. 1991; 17(5): 635-652.
- [31] Lopez de Bertodano M, Lahey RT, Jones OC. Turbulent bubbly two-phase flow data in a triangular duct. *Nuclear Engineering and Design*. 1994; 146(1-3): 43-52.
- [32] Rusdin A. Computation of turbulent flow around a square block with standard and modified k- ϵ turbulence models. *International Journal of Automotive and Mechanical Engineering*. 2017; 14(1): 3938-3953.
- [33] Ahmed SU, Arora R, Parkash O. Flow characteristics of multiphase glass beads-water slurry through horizontal pipeline using Computational Fluid Dynamics. *International Journal of Automotive and Mechanical Engineering*. 2019; 16(2): 6605-6623.
- [34] Fluent A. 15.0: Theory Guide, ANSYS, Inc, Canonsburg, PA. 2013.
- [35] Troshko AA, Hassan YA. A two-equation turbulence model of turbulent bubbly flows. *International Journal of Multiphase Flow*. 2001; 27(11): 1965-2000.
- [36] Singh NK. Simulation of flow over a rotationally oscillating square cylinder at low Reynolds numbers. *International Journal of Automotive and Mechanical Engineering*. 2019; 16(1): 6368-6385.
- [37] Mallard WG, Linstrom PJ. NIST Chemistry WebBook. NIST Standard Reference Database. 1998; 69.
- [38] Hardik BK, Prabhu SV. Boiling pressure drop and local heat transfer distribution of helical coils with water at low pressure. *International Journal of Thermal Sciences*. 2017; 114: 44-63.
- [39] Kurnia JC, Sasmito AP. Heat transfer performance of non-circular coiled tubes - Research summary, challenges and directions. *International Journal of Automotive and Mechanical Engineering*. 2016; 13(3): 3710-3727.
- [40] Kurnia JC, Sasmito AP, Shamim T, Mujumdar AS. Numerical investigation of heat transfer and entropy generation of laminar flow in helical tubes with various cross sections. *Applied Thermal Engineering*. 2016; 102: 849-860.
- [41] Cioncolini A, Santini L, Ricotti ME. Subcooled and saturated water flow boiling pressure drop in small diameter helical coils at low pressure. *Experimental Thermal and Fluid Science*. 2008; 32(6): 1301-1312.